JACS
JOURNAL OF THE AMERICAN CHEMICAL SOCIETY
pubs.acs.org/JACS
Article

High-Performance Humidity Sensing in π-Conjugated Molecular Assemblies through the Engineering of Electron/Proton Transport and Device Interfaces

Nicholas Turetta, Marc-Antoine Stoeckel, Rafael Furlan de Oliveira, Félix Devaux, Alessandro Greco, Camila Cendra, Sara Gullace, Mindaugas Gicevičius, Basab Chattopadhyay, Jie Liu, Guillaume Schweicher, Henning Sirringhaus, Alberto Salleo, Mischa Bonn, Ellen H. G. Backus, Yves H. Geerts, and Paolo Samorì*

Cite This: J. Am. Chem. Soc. 2022, 144, 2546–2555

ABSTRACT: The development of systems capable of responding to environmental changes, such as humidity, requires the design and assembly of highly sensitive and efficiently transducing elements. Such a challenge can be mastered only by disentangling the role played by each component of the responsive system, thus ultimately achieving high performance by optimizing the synergistic contribution of all functional elements. Here, we designed and synthesized a novel [1]benzothieno[3,2-*b*][1]-benzothiophene derivative equipped with hydrophilic oligo-ethylene glycol lateral chains (OEG-BTBT) that can electrically transduce subtle changes in ambient humidity with high current ratios (>10^4) at low voltages (2 V), reaching state-of-the-art performance. Multiscale structural, spectroscopical, and electrical characterizations were employed to elucidate the role of each device constituent, viz., the active material's BTBT core and OEG side chains, and the device interfaces. While the BTBT molecular core promotes the self-assembly of (semi)conducting crystalline films, its OEG side chains are prone to adsorb ambient moisture. These chains act as hotspots for hydrogen bonding with atmospheric water molecules that locally dissociate when a bias voltage is applied, resulting in a mixed electronic/protonic long-range conduction throughout the film. Due to the OEG-BTBT molecules' orientation with respect to the surface and structural defects within the film, water molecules can access the humidity-sensitive sites of the SiO_2 substrate surface, whose hydrophilicity can be tuned for an improved device response. The synergistic chemical engineering of materials and interfaces is thus key for designing highly sensitive humidity-responsive electrical devices whose mechanism relies on the interplay of electron and proton transport.

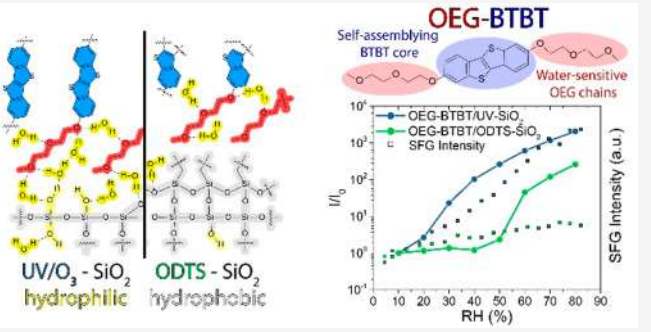

INTRODUCTION

Achieving precise control over the chemistry of our environment is key for well-being and for guaranteeing high standards for industrial and technological processes.[1] Environmental humidity is one of the ambient parameters that can severely affect the shelf life of goods and the efficiency of large-scale industrial systems, e.g., the correct functioning of machinery, and it needs to be finely controlled in surgery rooms in hospitals. Humidity can also unpredictably influence the outcome of laboratory experiments, as it modifies the reactivity and various properties of materials at the nanoscale. Too high or too low relative humidity (RH), its abrupt or slow fluctuations, and its broad or narrow variations can also significantly affect the performance and stability of electronic devices, for example, for energy production, storage, and conversion.[2−4] Thus, the subtle control of the ambient humidity, especially its useful and rational exploitation, is pivotal for modern and sustainable technologies in diverse fields.

The development of humidity-responsive materials and technologies has experienced a rapid expansion over the past few years.[5,6] Applications typically include sensors for humidity monitoring and humidity-driven actuators.[5] Materials and systems designed to smartly respond to humidity changes frequently undergo a modification of their size (viz., swelling or shrinking) due to chemical/physical processes triggered by water uptake or release via evaporation.[5] Very frequently

Received: September 24, 2021
Published: February 7, 2022

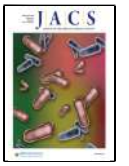

https://doi.org/10.1021/jacs.1c10119
J. Am. Chem. Soc. 2022, 144, 2546−2555

though, electrical control or readout is an extrinsic element of such materials and systems, being implemented only *a posteriori*.[5] On the other hand, some other technologies are designed to display high sensitivity in their electrical response to humidity changes as a result of electrical processes (ionic or electronic).[7] Importantly, the direct electrical transduction enables facile device integration with other electronic components to develop advanced applications.[6]

Humidity-responsive materials and devices must be rationally designed both to maximize physical interactions with atmospheric water molecules and to efficiently translate such interactions into useful electrical responses. Humidity responsiveness can be granted to organic, inorganic, and hybrid materials via *ad hoc* synthesis of functional systems or functionalization with appropriate chemical groups.[7] Functional humidity-sensitive moieties, which act as active sites for interactions with atmospheric water molecules, include hydroxyl, carboxyl, and nitro groups, quaternary ammonium, sulfonate, or phosphonium salts, and vinyl alcohol and ethylene glycol units.[8] Electrical transduction occurs by exploiting the ability of such functionalized materials to transport or accumulate charges (electronic or ionic species), whose behavior is influenced by their interaction with atmospheric water molecules. In this framework, humidity-responsive materials and devices can be designed and optimized to feature high performance via the in-depth understanding of the influence of the adsorbed water on such electronic/ionic conduction processes.

Here, we report on the engineering of a small conjugated molecule capable of self-assembling into semiconducting thin crystalline films possessing controlled interfaces with the environment to maximize physical interactions with atmospheric water and leverage electrical transduction. Toward this end, a novel molecular building block was designed to combine two key characteristics for the development of highly sensitive and reversible humidity-responsive chemiresistors: (i) a conjugated benzothienobenzothiophene (BTBT) core and (ii) methyl-terminated diethylene glycol side chains, hereinafter referred to as oligoethylene glycol (OEG) groups (see Figure 1a). The BTBT cores self-assemble to form crystalline films displaying a highly delocalized electronic structure capable of efficient electronic transport at long distances.[9,10] The OEG side chains, in turn, introduce hygroscopic properties to the host semiconducting core, enabling a fine sensitivity to subtle humidity changes and a mixed electron–ion transport.[11] Finally, the use of SiO_2 as device support makes it possible to master the substrate surface properties. In conjunction with the proper electrode geometry, these properties are instrumental in leveraging the responsiveness to water molecules and transducing effects.

The fabricated OEG-BTBT chemiresistors displayed reversible current changes up to a factor of $\sim 2 \times 10^4$ within the 10–80% RH range when thin films of optimized thickness are deposited on hydrophilic SiO_2 substrates having a top-contact electrode configuration. Such humidity-dependent response outperforms that presented by thin-film devices based on various functionalized small conjugated organic molecules.[12−17] The device response is completely reversible upon RH increase and decrease, exhibiting far improved stability with respect to its PEG-based counterpart.

Multiscale structural, spectroscopical, and electrical characterizations allowed shedding light on the role played by each responsive part of the device (i.e., the active material's BTBT core and OEG side chains, the chemiresistor top and bottom interfaces, its resistive and capacitive contributions, and electrode configuration). Our results reveal that OEG-BTBT chemiresistor operation is based on mixed electronic/protonic

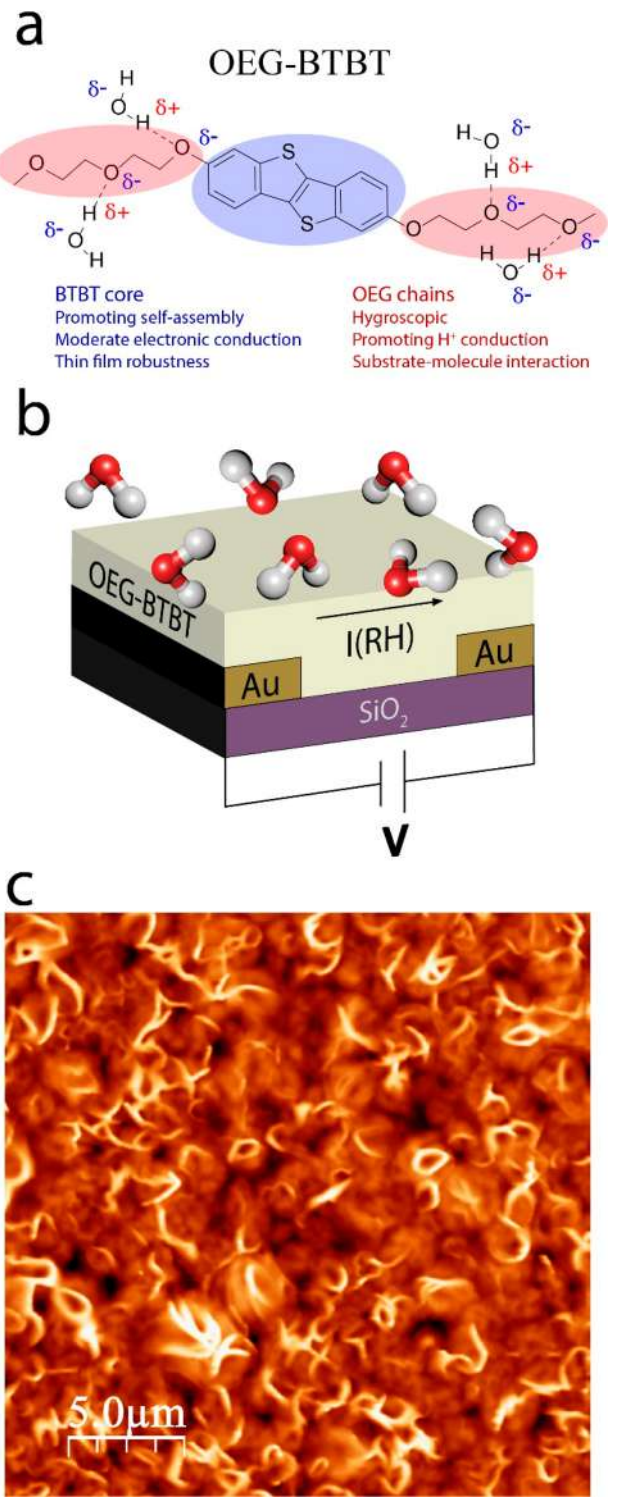

Figure 1. (a) Chemical structure of the OEG-BTBT molecule and its interaction with atmospheric water molecules via H-bonding interactions. (b) Sketch of the OEG-BTBT humidity-responsive chemiresistor. The RH-sensitive device current I(RH) is recorded upon application of a constant DC bias (V). (c) AFM height image of the spin-cast OEG-BTBT film surface deposited on SiO_2. Z-scale: 380 nm, R_{RMS}: 67 nm.

https://doi.org/10.1021/jacs.1c10119
J. Am. Chem. Soc. 2022, 144, 2546−2555

(H^+) accumulation and transport derived from the adsorbed atmospheric water, which is synergistically favored by employing thin films deposited on hydrophilic SiO_2 substrates. In stark contrast, hole-conducting BTBT cores decorated with alkyl side chains (C8-BTBT) show no significant humidity response, which endorses the key role played by the hygroscopic OEG moieties. These fundamental insights enable the optimal design of highly sensitive humidity-responsive electrical devices via synergistic chemical engineering of materials and interfaces based on a combined electronic and protonic transport.

RESULTS AND DISCUSSION

The as-synthesized OEG-BTBT molecules (Figure 1a) were deposited as thin films onto SiO_2 test patterns, as shown in Figure 1b. Details on the OEG-BTBT synthesis and characterization employing X-ray diffraction (XRD), ^1H and ^{13}C NMR, UV−vis, IR, and mass spectroscopy are reported in Figures S1 to S7. The molecular film cast onto SiO_2 exhibits an average thickness of 90 nm (10 mg/mL in $CHCl_3$ for the OEG-BTBT suspensions, see Figure S8). The surface topography of OEG-BTBT crystalline thin films is characterized by the presence of lamellar structures (regions with heights exceeding 100 nm) organized in multiple small domains (Figure 1c). This peculiar topography is typical of other thienoacene thin films.[18] OEG-BTBT films exhibit an average root-mean-square roughness (R_{RMS}) of 50 ± 20 nm over an area of 25 μm × 25 μm. The film is continuous and homogeneous both on the test-pattern SiO_2 channel and on top of the Au electrode (Figure S9), which guarantees a responsive film with the same morphological characteristics over the whole device surface. However, since the moderate roughness of 90-nm-thick films hinders a further analysis of its structural properties, we imaged the surface topography of a thinner film with a nominal thickness of 6 nm (see Figure S2b). Here, we note that the interfacial layer is characterized by the platelet morphology that is commonly observed for BTBT derivatives.

The response of OEG-BTBT chemiresistors to humidity changes was evaluated by applying a small 2 V bias step while monitoring the device current I(RH) for an interval of 10 s at different RH levels (Figure 2a). The application of short voltage steps reduces current-drifting problems observed in organic electronic devices operating at prolonged constant bias application,[19] especially in the presence of elevated humidity.[20] Alongside, pulsed measurements are more technologically relevant for sensing as less power is consumed when compared to long-term continuous operation. In our case, upon a 2 V bias step, we observe a short initial capacitive transient current,[21] followed by a near steady-state response at different RH (Figure 2a). Details on the chemiresistor transient response are shown in Figure S10.

As displayed in Figure 2a, the measured currents are noisy for RH < 30%, reaching the experimental signal detection limit (DL) of ca. 5 pA at RH ≈ 10%. As RH increases, the chemiresistor steady-state current also increases. Upon reverse voltage sweep measurements (Figure 2b), the device I−V characteristics within a ±2 V window exhibit a marked hysteresis as RH increases. This hysteresis increases in magnitude while increasing the voltage scan rate (from 440 to 2410 mV/s, Figure S11), indicating a capacitive contribution in the device response likely due to water-related charge-trapping effects at the proton blocking Au electrodes or at the dielectric interface.[22]

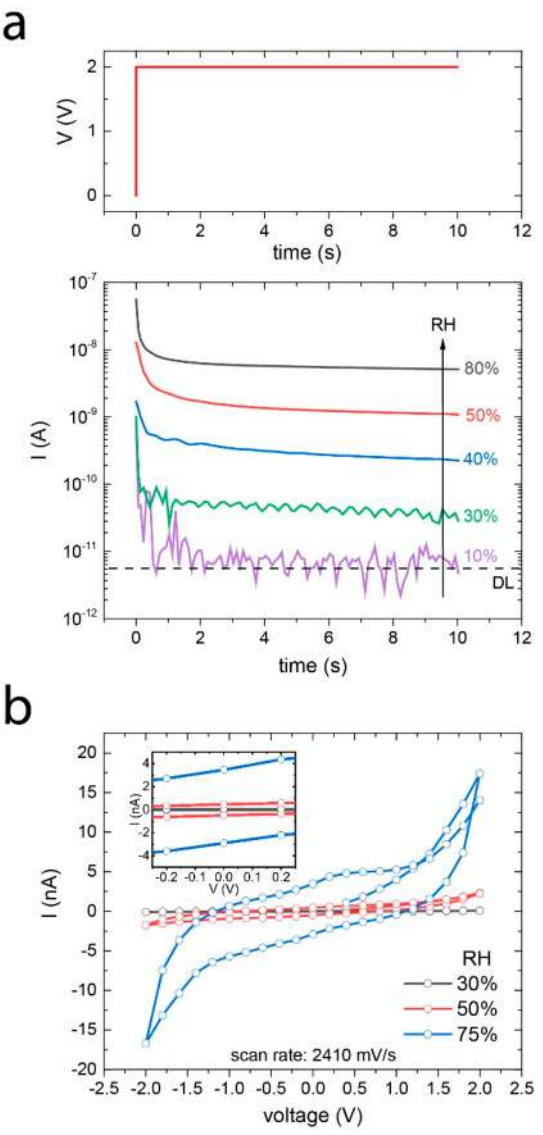

Figure 2. Electrical performance of RH-responsive chemiresistors (bottom-contact configuration). (a) Voltage bias stimulus (top) and respective chronoamperometric response of OEG-BTBT devices fabricated onto bare, nontreated SiO_2 at different RH levels (bottom). The current detection limit (DL) is indicated with a dashed black line. (b) I−V curves of OEG-BTBT onto bare SiO_2 measured at different RH at fast sweep rates (2410 mV/s). Inset: Zoomed hysteric I−V response at small biases. Device channel length: L = 5 μm.

Our devices have also shown to react quickly and reversibly to short (Figure 3a) and long (Figure 3b) intermittent RH changes. We found response (τ_g) and recovery times (τ_d) of ∼100−500 ms, depending on the device geometry (see Section 4 of the SI), which is fast enough for most humidity-sensing applications. In addition, the exposure of our chemiresistors to vapors of different volatile solvents (i.e., ethanol, methanol, ethyl ether) only produces a minor current response (Figure S12). This electrical behavior indicates a high selectivity for water molecules, which are responsible for the observed current increase with the RH. Finally, to avoid slow charge-trapping phenomena that could lead to erroneous device metrics from I−V measurements performed with insufficient dwell time, we quantified the OEG-BTBT response by

https://doi.org/10.1021/jacs.1c10119
J. Am. Chem. Soc. 2022, 144, 2546−2555

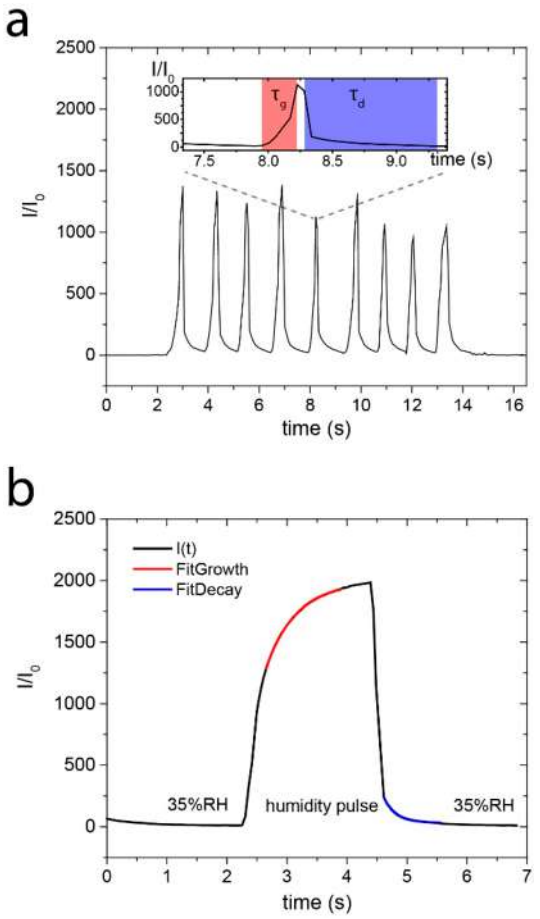

Figure 3. (a) Current response of the OEG-BTBT devices when exposed to a train of short (<1 s) humid air pulses during the application of a 2 V bias. Inset: Magnification of a pulse profile illustrating the method to estimate the device response (τ_g) and recovery (τ_d) times. (b) Current response to a single long (>1 s) pulse at RH ≈ 35%. The curves obtained by fitting of the $I(t)$ data during the growth (red) and the decay (blue) of the current are reported in the same graph.

measuring I(RH) at a constant |2 V| bias and at sufficiently long times (t > 5 s, I–t curve in Figure 2a).

For each transient I(RH) response, we separated the resistive and capacitive contributions (Figure S10) to extract current (I) and capacitance (C) values at different RH levels. Figure 4a portrays the device current response at each RH level (black curve) and the response of bare SiO_2 test patterns (gray curve). Each point in Figure 4a corresponds to the averaged current values measured during a time interval of 4 s (after stabilization, t > 5 s) for each $I(t)$ curve shown in Figure 2a. The measured current (I) was normalized with respect to the device initial response (I_0), i.e., at RH = 10%. Such a curve represents the chemiresistor current variations at precise RH levels quantified with a commercial humidity sensor (Sensirion SHT31 Smart Gadget). The change of the surrounding humidity from 10% to 80% resulted in a reversible current modulation in OEG-BTBT devices that spanned 3 orders of magnitude ($I/I_0 \approx 10^3$). Substantial hysteresis has not been observed for such devices (bottom-contact (BC) configuration and short channel, L = 5 μm) operating under pulsed bias, as the current at a given RH lies within the mean values of both the forward and backward curves.

Our state-of-the-art humidity-sensitive two-terminal devices have several advantages over a three-terminal (transistor) configuration by ensuring a simple fabrication process and a better sensing control/operation, as discussed in the SI (see Figure S14 and Section 5). In addition, it is fair to note that the role played by the substrate/active material interface is often neglected in the literature when investigating the performance of new materials for humidity-sensing applications (Table S1). Since thin-film devices are frequently supported on SiO_2 substrates, which possess an inherent moisture sensitivity,[23] we have investigated their role via surface modification through UV/ozone exposure[24] and alkylsilane functionalization.[25] This is an important measure to elucidate mechanisms and to optimize applications.[26] In addition, elucidating the role of the substrate avoids critical data misinterpretation, lack of understanding of the humidity-response mechanism, or even the overestimation of the device figures of merit.

Bare SiO_2 surfaces interact effectively with atmospheric water molecules[27] (Figure 4b), and water surface condensation is known to strongly influence the SiO_2 electrical properties.[26,28] Here, we observed that bare SiO_2 substrates reversibly respond to RH changes, yet with a response being significantly inferior to that of OEG-BTBT chemiresistors, i.e., $I/I_0 \leq 10$ in the 10–80% RH range (Figure 4a, light gray curves). Additionally, the chemiresistors exhibit an excellent reversibility when various bias voltage pulses are serially applied, as shown in Figure S13 by the I(RH) transient curves consecutively collected at ±2 V. Upon augmenting the hydrophilicity of the SiO_2 surface by means of UV/ozone treatment, we observed an increase in the responsivity of both the bare substrate (due to the increased number of exposed water-sensitive surface groups) and the OEG-BTBT devices (Figure 4c). In particular, when the substrate wettability is enhanced via UV/ozone treatment (water contact angle (CA) < 10°), followed by the OEG-BTBT deposition, the chemiresistor response increases by a factor of ca. 5 compared to devices fabricated on bare SiO_2 (CA ≈ 55°). OEG-BTBT devices fabricated onto OH-rich SiO_2 surfaces attain $I/I_0 > 10^3$ for RH increasing from 10% to 80% (Figure 4c). Conversely, the octadecyltrichlorosilane (ODTS) treatment of SiO_2 (CA ≈ 110°) gives rise to a significantly reduced response of both OEG-BTBT-coated and uncoated substrates, as water molecules can only bind to the surface defects remaining on the surface of ODTS-treated SiO_2. In both cases, detectable current signals are recorded only above RH > 40%. By and large, the control of the wettability at the interface between the substrate and the active material has a dramatic influence on the overall performance of OEG-BTBT chemiresistors, demonstrating the major benefits brought by the synergistic effect of a hygroscopic molecular film supported on a humidity-responsive substrate.

The substrate wettability is also known to influence the depth distribution of water adsorbed across hydrophilic thin films.[29] Thus, to further evaluate the role played by the SiO_2/OEG-BTBT interface, sum-frequency generation (SFG) measurements were performed at variable RH on treated substrates. SFG is a nonlinear optical technique that provides a signal only for non-centrosymmetric systems.[30] At an interface, the symmetry is naturally broken, making the method interface-specific. Here, we monitored the water present at the interface between SiO_2 and the OEG-BTBT film by measuring the integrated SFG signal from the O–H stretching mode (~3300 cm^{-1}) as a function of RH (Figure 4d and

https://doi.org/10.1021/jacs.1c10119
J. Am. Chem. Soc. 2022, 144, 2546–2555

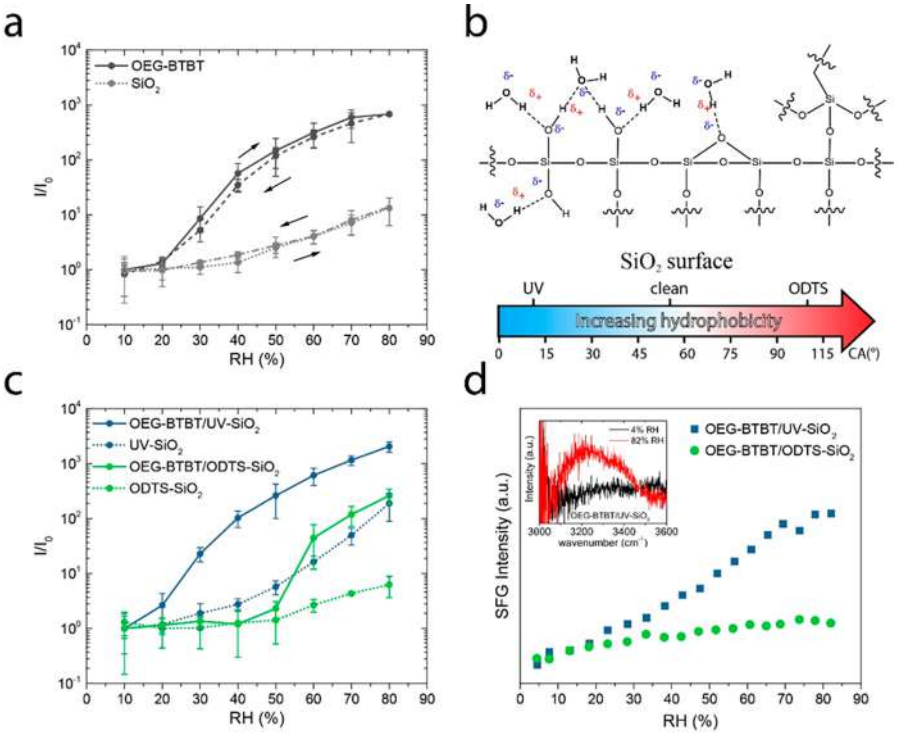

Figure 4. (a) Normalized current (I/I_0) response as a function of RH for bottom-contact OEG-BTBT onto SiO_2 devices (solid dark grey line) and bare SiO_2 (dotted light gray line) samples. The arrows illustrate the reversibility of the chemiresistor response upon the RH increase and following decrease. Dashed and dash-dotted lines indicate values obtained while decreasing the RH (see arrow direction). (b) H-bond interactions of water molecules with silanol and Si−O−Si groups of the SiO_2 surface. (c) Current response of OEG-BTBT devices fabricated on treated SiO_2 (UV/ozone and ODTS, solid lines) and bare substrates (dotted lines). For OEG-BTBT/ODTS-SiO_2 and ODTS-SiO_2 devices, the current reaches the instrumental DL at RH ≤ 40%. (d) Sum frequency generation (SFG) integrated intensity of the 3300 cm^{-1} O−H stretching band of 50 nm OEG-BTBT thin films on UV-SiO_2 and ODTS-SiO_2 substrates. Inset: SFG spectrum of the OEG-BTBT/UV-SiO_2 interface at low (4%) and high (82%) RH. Current values and error bars in (a) and (c) correspond to the average response and respective standard deviation values determined from $n \geq 3$ tested chemiresistors. Device channel length: $L = 5$ μm. RH range: 10−80%. Voltage bias applied: 2 V.

inset). For this purpose, 50-nm-thick OEG-BTBT films were prepared onto quartz substrates of optical grade modified by either UV/ozone or ODTS. We observed that the different surface wettability indeed affects the quantity of water molecules adsorbed at the substrate/molecular film interface, as shown by the increased SFG signal of samples prepared onto hydrophilic substrates (Figure 4d inset). In addition, the integrated SFG signal for OEG-BTBT films (in blue) onto hydrophilic substrates increases substantially more upon RH increase compared to films on hydrophobic SiO_2 (in green, Figure 4d). Water molecules are known to adsorb at the SiO_2 surface silanol sites,[31] thereby forming a network driven by H-bonding only.[32] This process results in a uniform water layer of growing thickness (a few monolayers thick) at increasing RH.[33] The amount of water that reaches such an interface via permeation through the organic film governs the device I(RH) response (Figure 4a) likely due to a larger and more efficient network of water molecules for the percolation of H^+ upon the voltage bias.[34] The formation of sites for proton conduction occurs spontaneously at room temperature, as water is partially dissociated into chemisorbed H and OH on Si atoms at the SiO_2 and Si(100) surfaces.[35] This explains why OEG-BTBT films deposited onto hydrophilic SiO_2 exhibit better humidity-sensing performance than those based on hydrophobic substrates.

Electrical transduction of humidity changes is strongly dependent on the nature of the humidity-sensitive material, which dictates the dominant electrical process (conduction/accumulation) and related charged species (electronic or ionic).[6,7] OEG-BTBT films at elevated RH display a mixed electronic/protonic (H^+) conductivity (Figure S19). Thus, to cast light onto the dominant electrical processes in our OEG-BTBT devices (charge transport and/or accumulation), we also evaluated the capacitive contribution contained in the transient I(RH) response of each sample (Figure 2b). The normalized capacitance (C/C_0) of OEG-BTBT films and noncoated substrates as a function of RH is shown in Figure 5a. Each point of the curve corresponds to C/C_0, where C is calculated by dividing the amount of charge stored (Q) in the sample at a given RH by the applied voltage (see Figure S10 for details). C_0 is determined at 10% RH.

Figure 5a reveals that the capacitive response of OEG-BTBT films is superior to that of bare substrates as the RH increases. Such a capacitive behavior clearly indicates the H^+ charge storage ability of OEG-BTBT films, which agrees with their hysteric $I-V$ characteristics observed at elevated RH (Figure 2b). The C/C_0 ratio for OEG-BTBT films increases for RH > 20%, reaching approximately 3×10^2 at the maximum probed humidity (viz., 80%). Remarkably, the C/C_0 ratio of OEG-BTBT chemiresistors exceeds that of similar capacitive thin-film devices based on small organic molecules functionalized with OEG chains,[15] indicating a gain of performance in our devices due to their engineered characteristics. By contrast, the response of OEG-BTBT-free substrates is limited to $C/C_0 \leq 20$. In Figure 5a, we also note that above 60% RH the OEG-BTBT capacitive response is almost independent of the

https://doi.org/10.1021/jacs.1c10119
J. Am. Chem. Soc. 2022, 144, 2546−2555

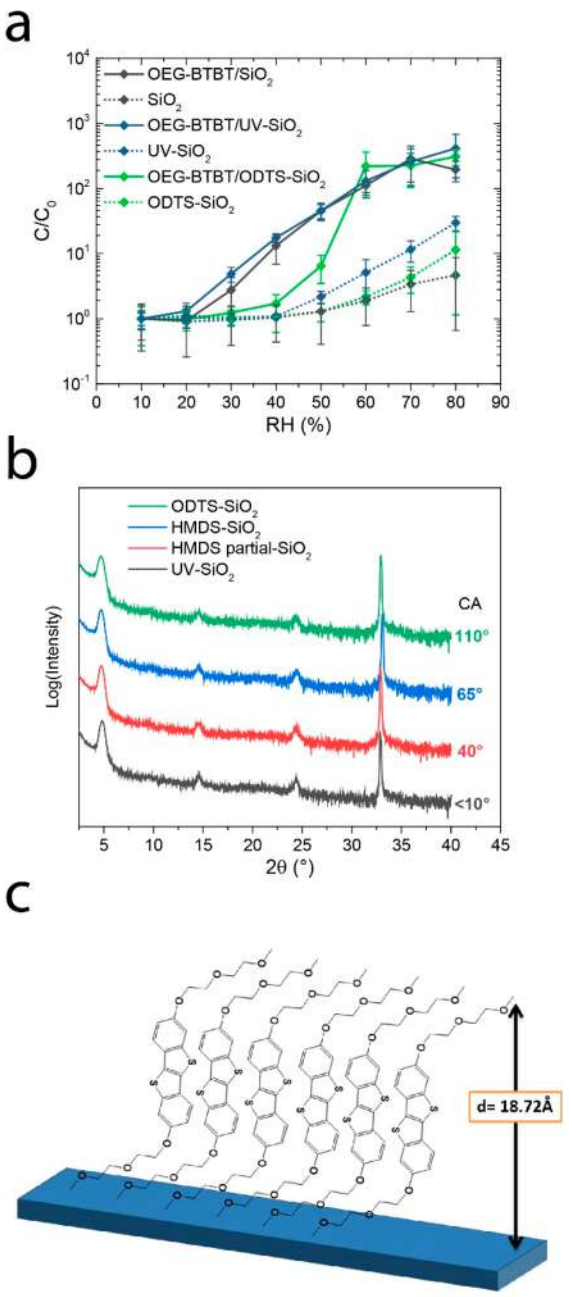

Figure 5. (a) Normalized capacitance (C/C_0) curves for BC OEG-BTBT/SiO_2 devices (solid lines) and OEG-BTBT-free substrates (dotted lines). Error bars correspond to standard deviation values acquired for $n \geq 3$ devices. Device channel length: $L = 5$ μm. RH range: 10−80%. Voltage bias applied: 2 V. (b) Out-of-plane XRD spectra collected for OEG-BTBT thin films spin-cast on modified SiO_2 (water contact angle (CA) values denote wettability for the respective surface treatments). (c) OEG-BTBT molecular structure and surface arrangement on SiO_2 indicating an interlayer spacing (d) of 18.72 Å (for crystalline regions formed on hydrophobic substrates), calculated from XRD measurements in (b).

substrate surface characteristics. This suggests that the entrapment of atmospheric water molecules and related charge storage in the device both depend primarily on the OEG-BTBT film properties, while charge conduction is interface-sensitive (Figure 5c).

When self-assembled molecular materials respond to humidity changes, the rationalization of the response mechanisms is often considered from a structural perspective.[14,36] To gain insight into a potential structural change resulting from the humidity variation at the supramolecular level, we performed grazing-incidence wide-angle X-ray scattering (GIWAXS) measurements. The results revealed that the OEG-BTBT crystalline structure is insensitive to the changes of humidity level (Figure S15). In fact, neither the in-plane nor the out-of-plane GIWAXS patterns presented appreciable peak shifts as a function of RH, suggesting that the self-assembling BTBT core offers major crystallographic stability upon changing the surrounding RH. Therefore, the observed humidity responsiveness of OEG-BTBT devices cannot be explained by the occurrence of structural changes that would cause variations of the $\pi-\pi$ stacking distance and related current changes.[14,36] A gradual variation of surface hydrophilicity was carried out with the aim of unraveling possible modifications of the OEG-BTBT crystal structure arising from the substrate treatment. XRD analysis indicates an interlayer spacing (d) of ca. 18.72 Å for the OEG-BTBT crystalline regions formed on hydrophobic surfaces (ODTS- and hexamethyldisilazane- (HMDS) functionalized SiO_2) and of ca. 18.26 Å onto hydrophilic UV/ozone-treated substrates (Figure 5b). These molecular height values at the solid state are in good agreement with the 18.5 ± 0.9 Å step terrace height determined from the AFM topography imaging of a 6-nm-thick film of spin-casted OEG-BTBT on SiO_2 (see Figure S2b).

This accounts for only a 2.5% reduction of d-spacing when changing from hydrophobic to hydrophilic substrate surfaces. Such a minute structural difference in the bulk of OEG-BTBT films cannot be responsible for the pronounced humidity response observed. No other substantial differences are found in the XRD spectra upon the various surface treatments. Finally, from the calculated d-spacing, the expected OEG-BTBT molecular arrangement on the surface is concluded to be the vertical standing as depicted in Figure 5c. Within this packing motif, some humidity-sensitive OEG chains of our molecule are in proximity to the substrate surface, enhancing water interactions at the interface. The comparison of the thin-film XRD peaks in Figure 5b with those of the powder XRD spectrum in Figure S2 highlights that the thin film exhibits a strong preferential orientation related to the planes corresponding to the molecule packed in this arrangement. This may explain the intense current and capacitance responses (especially for RH > 50%) of OEG-BTBT films even when ODTS-treated surfaces are employed as water molecules easily permeate the polycrystalline thin film through grain boundaries. Water entrapment at the substrate−semiconductor interface may also be the reason for the peculiar curve shape and marked response of OEG-BTBT with respect to that of the uncoated ODTS-treated substrates (Figure 5c).

The chemiresistor response is also shown to depend on the electrode geometry (TC vs BC, Figure S17), as expected by considering the current distribution across thin-film devices.[37] Considering a H^+ transport contribution, the conductivity of films can be expected to scale with both the RH and the thickness of the H^+-conductive film, with devices incorporating thicker layers showing larger conductivities.[38] By optimizing the device geometry and electrode configuration, we could achieve an I/I_0 ratio around 2×10^4 by employing TC OEG-BTBT in the 10−80% RH range. The responsivity of our chemiresistors outperforms that of numerous humidity-sensitive resistive devices based on a variety of conjugated

https://doi.org/10.1021/jacs.1c10119
J. Am. Chem. Soc. 2022, 144, 2546−2555

small molecules (see Table S2). Therefore, high performance in humidity-responsive devices is achieved by synergistically combining a material (OEG-BTBT) designed to be humidity responsive (via a mixed electron/proton accumulation and transport) with functionalized substrates and the most favorable electrode configuration.

Given the crucial role of the hydrophilic lateral chain groups, we compared the electrical response of OEG-BTBT with that of benchmark semiconductor alkyl-functionalized C8-BTBT. Ethylene glycol-functionalized polymers are known to present mixed ionic/electronic conduction,[39] and electrochemical impedance spectroscopy (EIS) at high RH (>90%) is a routine technique for the characterization of these mixed conductors.[40] Here, we observed that at low humidity (RH ≈ 10%) OEG-BTBT and C8-BTBT films behave similarly (Figure S19 and Table S3), exhibiting a response predominantly capacitive with a high-resistance contribution (conductivity $\sigma_e \approx 10^{-5}-10^{-6}$ S/cm). As RH increases to ∼97%, the behavior of the two devices differs significantly and the mixed ionic/electronic conduction properties of OEG-BTBT films manifest (Figure S19). While the increase of humidity only slightly modifies the electronic conduction properties of C8-BTBT films ($\sigma_e \approx 1 \times 10^{-4}$ S/cm), the OEG-BTBT samples exhibit a low-frequency (<kHz) EIS response characteristic of transport of heavy species (ions).[40,41]

As this behavior is observed only in humid conditions (and not at RH ≈ 10%) and OEG-BTBT does not possess structural ionic groups, we attribute such ionic conduction to dissociated H^+ from atmospheric water molecules at the ethylene glycol moieties of OEG-BTBT that are transported upon the effect of the voltage bias.[39,42] We found an ionic conductivity of $\sigma_i \approx 2 \times 10^{-3}$ S/cm, which is similar to the values reported for other organic H^+ conductors.[21] Further DC experiments on such samples reveal that C8-BTBT samples are significantly less sensitive to RH changes than OEG-BTBT films (Figure S20). C8-BTBT devices exhibit a predominant hole-transporting characteristic, and an increase of humidity only leads to instabilities and degradation of the carrier mobility.[43] The observed high-performance humidity responsiveness of OEG-BTBT can therefore be intimately associated with the mixed electronic/protonic conductivity that governs the electrical response of such films.

We also compared the response of our synthesized BTBT derivative with that of linear PEG thin films (Figure S21). PEG is known to exhibit a current response that increases in magnitude upon water uptake,[44] provided that a proton/ion source is present within the film.[45] PEG is indeed widely employed in proton exchange membranes, as it facilitates proton conduction in humid environments by providing an ion percolation path.[46,47] In addition, PEG's repeat unit is chemically identical to OEG side groups in OEG-BTBT, making it the perfect prototypical system for comparative analysis. OEG-BTBT and PEG were spin-cast on UV/ozone-treated BC interdigitate electrodes test patterns from $CHCl_3$ (10 mg/mL) to form thin films with an average thickness of 80−90 nm. Their humidity response also shows an initial capacitive current transient followed by a near-steady-state response within the first 10 s of monitoring (Figure S21). Although the two compounds display a similar overall current change within the considered RH range (Figure 6), their behavior differs significantly during such a variation (Figure S18). The I(RH) curve of PEG/UV-SiO_2 shows a similar trend

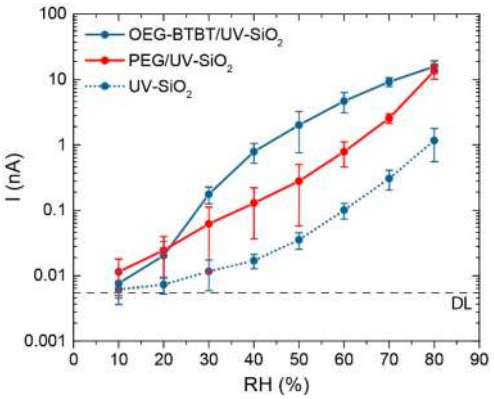

Figure 6. Absolute current curves as a function of RH for OEG-BTBT and PEG thin-film BC devices on UV-treated SiO_2 substrates (channel L = 5 μm). The electric response for the noncoated treated substrate is also reported. The dashed line indicates the experimental detection limit. Error bars correspond to the standard deviation acquired for $n \geq 3$ devices. Device channel length: L = 5 μm. RH range: 10−80%. Voltage bias applied: 2 V.

to that of noncoated UV-treated SiO_2, with higher absolute current values.

This finding suggests that more water molecules can be hosted within the PEG film than those that could be adsorbed onto the bare SiO_2 surface. Figure 6 reveals that the OEG-BTBT/UV-SiO_2 and the PEG/UV-SiO_2 curves exhibit similar current values at very low (<20%) and very high RH (80%), but a different behavior at intermediate RH (20−50%). Within this range, OEG-BTBT/UV-SiO_2 samples display the largest sensitivity (compared to PEG/UV-SiO_2 and bare UV-SiO_2), which can be ascribed to the efficiently packed OEG groups in OEG-BTBT films. Indeed, thin films exhibiting molecularly oriented structures are being extensively studied as promising candidates for improved proton conduction.[48] Further evidence of the analogies in OEG-BTBT and PEG electrical behavior is given by a comparative study among these compounds and C8-BTBT. $I-V$ measurements of BC devices (UV-SiO_2 substrates) with comparable thin-film thickness (∼100 nm) were collected by sweeping the voltage at ∼2400 mV/s within a ±2 V window at varied RH (Figure S18). While the $I-V$ curves of OEG-BTBT and PEG devices are similar in shape (and in intensity at very high RH) and characterized by a strong capacitive contribution, C8-BTBT devices exhibited almost negligible hysteresis as the forward and backward $I-V$ curves cross at 0 V. Since the charge transport in C8-BTBT is expected to be purely electronic while for PEG it is purely protonic, we can infer that the protonic character prevails in OEG-BTBT devices.

Finally, quantifying the chemiresistor sensitivity, i.e., the I(RH) curve slope, is challenging, as OEG-BTBT films do not exhibit a current response with a well-defined trend (e.g., linear, logarithmic, exponential). Previous surface conductivity measurements on bare SiO_2 showing a response very similar to that of our SiO_2 samples have revealed three regimes corresponding to the structural evolution of the water layer condensing at different RH (namely, ice-like, transition, and water-like structures).[26,33] The same rationalization, however, seems not to be applicable to the response of OEG-BTBT chemiresistors. Additionally, the I(RH) data for PEG-based devices can be approximately modeled by an exponential function within the studied RH range, closely resembling a

https://doi.org/10.1021/jacs.1c10119
J. Am. Chem. Soc. 2022, 144, 2546−2555

type-3 sorption isotherm.[44,49] This simplified scenario does not apply here for OEG-BTBT films, where a detailed determination of how water interacts with OEG-BTBT and the derivation of a simple expression for the calibration curve using such devices become very challenging. Regarding structural stability, PEG thin films are known to undergo a phase change into gel-like structure at RH > 80%,[50] thus suffering from a critical dewetting when exposed to elevated humidity (Figure S22a–d).[44] On the other hand, OEG-BTBT displays remarkable stability, as no macroscopic changes are detected upon exposure to high RH (Figure S22e–h). The superior robustness of OEG-BTBT films is further corroborated by small current variations observed when the samples are stored at elevated RH for long periods (>20 h), while the performance of PEG-based devices deteriorates quickly (Figure S23).

CONCLUSION

Highly humidity-sensitive chemiresistors based on thin films of a novel hygroscopically engineered conjugated small molecule (OEG-BTBT) have been devised. To combine enhanced humidity responsiveness with efficient electrical transduction, we have designed and synthesized a novel semiconducting BTBT molecule with mixed electron/proton-conducting behavior. Thanks to the combination of EIS measurements and the comparative studies performed on PEG and C8-BTBT, clear evidence that proton transport dominates the response of OEG-BTBT at high humidity was provided. When OEG-BTBT is spin-cast onto SiO_2 substrates having appropriate electrode configuration, it results in self-assembled semiconducting molecular films that electrically respond to variations of RH outperforming several other similar devices. The conductivity of our chemiresistors changes up to a factor of $\sim 2 \times 10^4$ within the 10–80% RH range when built onto hydrophilic, UV/ozone-treated SiO_2 substrates in an optimized electrode configuration. The device response is fully reversible to increasing and decreasing ambient RH and shows a remarkable stability when exposed to elevated humidity (>90%). A multiscale structural, spectroscopical, and electrical characterization of our samples allowed us to identify that such a performance derives from a synergistic combination of the material's properties (i.e., its semiconducting core and hygroscopic functional side chains), the chemiresistor interfaces and device configuration (position with respect to the film surface, channel length, and thin-film thickness). This synergy allows OEG-BTBT thin-film devices to effectively transduce RH changes with improved sensitivity, thus rendering them suitable for a multitude of water-responsive electronic applications.

ASSOCIATED CONTENT

Supporting Information

The Supporting Information is available free of charge at https://pubs.acs.org/doi/10.1021/jacs.1c10119.

Synthetic procedures and characterization of OEG-BTBT; photographs of OEG-BTBT suspensions; SEM imaging, SFG and GIWAXS measurements, additional electrical characterization of the OEG-BTBT thin-film devices; EIS measurements, modeling, and comparison with C8-BTBT devices; device performance stability and additional comparison with PEG devices; AFM height images of OEG-BTBT, C8-BTBT, and PEG thin films; comparative tables of humidity-responsive devices from the literature (PDF)

AUTHOR INFORMATION

Corresponding Author

Paolo Samorì – *Université de Strasbourg, F-67000 Strasbourg, France;* orcid.org/0000-0001-6256-8281; Email: samori@unistra.fr

Authors

Nicholas Turetta – *Université de Strasbourg, F-67000 Strasbourg, France*

Marc-Antoine Stoeckel – *Université de Strasbourg, F-67000 Strasbourg, France*

Rafael Furlan de Oliveira – *Université de Strasbourg, F-67000 Strasbourg, France; Brazilian Nanotechnology National Laboratory (LNNano), Brazilian Center for Research in Energy and Materials (CNPEM), 13083-970 Campinas, São Paulo, Brazil*

Félix Devaux – *Laboratoire de Chimie des Polymères Faculté des Sciences, Université Libre de Bruxelles (ULB), 1050 Bruxelles, Belgium*

Alessandro Greco – *Max Planck Institute for Polymer Research, 55128 Mainz, Germany*

Camila Cendra – *Department of Materials Science and Engineering, Stanford University, Stanford, California 94305, United States;* orcid.org/0000-0003-1786-6540

Sara Gullace – *Université de Strasbourg, F-67000 Strasbourg, France;* orcid.org/0000-0002-1357-0526

Mindaugas Gicevičius – *Cavendish Laboratory, Department of Physics, University of Cambridge, Cambridge CB3 0HE, U.K.*

Basab Chattopadhyay – *Laboratoire de Chimie des Polymères Faculté des Sciences, Université Libre de Bruxelles (ULB), 1050 Bruxelles, Belgium; Department of Physics, Norwegian University of Science and Technology (NTNU), 7491 Trondheim, Norway;* orcid.org/0000-0001-5106-1880

Jie Liu – *Laboratoire de Chimie des Polymères Faculté des Sciences, Université Libre de Bruxelles (ULB), 1050 Bruxelles, Belgium;* orcid.org/0000-0002-1301-057X

Guillaume Schweicher – *Laboratoire de Chimie des Polymères Faculté des Sciences, Université Libre de Bruxelles (ULB), 1050 Bruxelles, Belgium*

Henning Sirringhaus – *Cavendish Laboratory, Department of Physics, University of Cambridge, Cambridge CB3 0HE, U.K.;* orcid.org/0000-0001-9827-6061

Alberto Salleo – *Department of Materials Science and Engineering, Stanford University, Stanford, California 94305, United States*

Mischa Bonn – *Max Planck Institute for Polymer Research, 55128 Mainz, Germany;* orcid.org/0000-0001-6851-8453

Ellen H. G. Backus – *Max Planck Institute for Polymer Research, 55128 Mainz, Germany; Department of Physical Chemistry, University of Vienna, 1090 Vienna, Austria;* orcid.org/0000-0002-6202-0280

Yves H. Geerts – *Laboratoire de Chimie des Polymères Faculté des Sciences, Université Libre de Bruxelles (ULB), 1050 Bruxelles, Belgium; International Solvay Institutes of Physics and Chemistry, 1050 Brussels, Belgium*

Complete contact information is available at: https://pubs.acs.org/10.1021/jacs.1c10119

https://doi.org/10.1021/jacs.1c10119
J. Am. Chem. Soc. 2022, 144, 2546–2555

Author Contributions

All authors have given approval to the final version of the manuscript.

Funding

The authors acknowledge the European Union's Horizon 2020 research and innovation program under the Marie Skłodowska-Curie grant agreements No. 811284 (UHMob) and No. 813036 (ULTIMATE). P.S. acknowledges the financial support from the Agence Nationale de la Recherche through the Labex project CSC (ANR-10-LABX-0026 CSC) within the Investissement d'Avenir program (ANR-10-120 IDEX-0002-02), the International Center for Frontier Research in Chemistry (icFRC) as the Institut Universitaire de France (IUF). Y.G. is thankful to the Belgian National Fund for Scientific Research (FNRS) for financial support through research projects BTBT no. 2.4565.11, Phasetrans no. T.0058.14, Pi-Fast no. T.0072.18, POLYGRAD no. 22333186, and 2D to 3D No. 30489208. Financial support from the French Community of Belgium (ARC no. 20061) is acknowledged. B.C. and G.S. acknowledge postdoctoral fellowship support from the FNRS. M.B. is grateful for financial support from the MaxWater initiative.

Notes

The authors declare no competing financial interest.

■ ACKNOWLEDGMENTS

We thank Prof. Fabio Biscarini (University of Modena/Italy) and Prof. Henrique L. Gomes (University of Coimbra/Portugal) for fruitful discussions, and Dr. Laura Schelhas and Dr. Stephanie Moffit (SLAC National Accelerator Laboratory) for technical assistance with the *in situ* humidity GIWAXS experiments. Some experimental activities were carried out at the Stanford Synchrotron Radiation Lightsource, a national user facility operated by Stanford University on behalf of the U.S. Department of Energy, Office of Basic Energy Sciences.

■ REFERENCES

(1) Fraden, J. Humidity and Moisture Sensors. In *Handbook of Modern Sensors: Physics, Designs, and Applications*; Fraden, J., Ed.; Springer International Publishing: Cham, 2016; pp 507−523.
(2) Li, D.; Borkent, E.-J.; Nortrup, R.; Moon, H.; Katz, H.; Bao, Z. Humidity Effect on Electrical Performance of Organic Thin-Film Transistors. *Appl. Phys. Lett.* **2005**, *86* (4), 042105.
(3) Chen, C.; Fuller, T. F. The Effect of Humidity on the Degradation of Nafion® Membrane. *Polym. Degrad. Stab.* **2009**, *94* (9), 1436−1447.
(4) Grossiord, N.; Kroon, J. M.; Andriessen, R.; Blom, P. W. M. Degradation Mechanisms in Organic Photovoltaic Devices. *Org. Electron.* **2012**, *13* (3), 432−456.
(5) Park, Y.; Chen, X. Water-Responsive Materials for Sustainable Energy Applications. *J. Mater. Chem. A* **2020**, *8* (31), 15227−15244.
(6) Farahani, H.; Wagiran, R.; Hamidon, M. N. Humidity Sensors Principle, Mechanism, and Fabrication Technologies: A Comprehensive Review. *Sensors* **2014**, *14* (5), 7881−7939.
(7) Chen, Z.; Lu, C. Humidity Sensors: A Review of Materials and Mechanisms. *Sens. Lett.* **2005**, *3* (4), 274−295.
(8) Najeeb, M. A.; Ahmad, Z.; Shakoor, R. A. Organic Thin-Film Capacitive and Resistive Humidity Sensors: A Focus Review. *Adv. Mater. Interfaces* **2018**, *5* (21), 1800969.
(9) Ruzié, C.; Karpinska, J.; Laurent, A.; Sanguinet, L.; Hunter, S.; Anthopoulos, T. D.; Lemaur, V.; Cornil, J.; Kennedy, A. R.; Fenwick, O.; Samorì, P.; Schweicher, G.; Chattopadhyay, B.; Geerts, Y. H. Design, Synthesis, Chemical Stability, Packing, Cyclic Voltammetry, Ionisation Potential, and Charge Transport of [1]Benzothieno[3,2-b][1]Benzothiophene Derivatives. *J. Mater. Chem. C* **2016**, *4* (22), 4863−4879.
(10) Schweicher, G.; Olivier, Y.; Lemaur, V.; Geerts, Y. H. What Currently Limits Charge Carrier Mobility in Crystals of Molecular Semiconductors? *Isr. J. Chem.* **2014**, *54* (5−6), 595−620.
(11) Schmode, P.; Savva, A.; Kahl, R.; Ohayon, D.; Meichsner, F.; Dolynchuk, O.; Thurn-Albrecht, T.; Inal, S.; Thelakkat, M. The Key Role of Side Chain Linkage in Structure Formation and Mixed Conduction of Ethylene Glycol Substituted Polythiophenes. *ACS Appl. Mater. Interfaces* **2020**, *12* (11), 13029−13039.
(12) Torsi, L.; Dodabalapur, A.; Cioffi, N.; Sabbatini, L.; Zambonin, P. G. NTCDA Organic Thin-Film-Transistor as Humidity Sensor: Weaknesses and Strengths. *Sens. Actuators B Chem.* **2001**, *77* (1), 7−11.
(13) Zhu, Z.-T.; Mason, J. T.; Dieckmann, R.; Malliaras, G. G. Humidity Sensors Based on Pentacene Thin-Film Transistors. *Appl. Phys. Lett.* **2002**, *81* (24), 4643−4645.
(14) Mogera, U.; Sagade, A. A.; George, S. J.; Kulkarni, G. U. Ultrafast Response Humidity Sensor Using Supramolecular Nanofibre and Its Application in Monitoring Breath Humidity and Flow. *Sci. Rep.* **2015**, *4* (1), 4103.
(15) Ali, S.; Jameel, M. A.; Gupta, A.; Langford, S. J.; Shafiei, M. Capacitive Humidity Sensing Performance of Naphthalene Diimide Derivatives at Ambient Temperature. *Synth. Met.* **2021**, *275*, 116739.
(16) Tahir, M.; Sayyad, M. H.; Clark, J.; Wahab, F.; Aziz, F.; Shahid, M.; Munawar, M. A.; Chaudry, J. A. Humidity, Light and Temperature Dependent Characteristics of Au/N-BuHHPDI/Au Surface Type Multifunctional Sensor. *Sens. Actuators B Chem.* **2014**, *192*, 565−571.
(17) Roslan, N. A.; Abu Bakar, A.; Bawazeer, T. M.; Alsoufi, M. S.; Alsenany, N.; Abdul Majid, W. H.; Supangat, A. Enhancing the Performance of Vanadyl Phthalocyanine-Based Humidity Sensor by Varying the Thickness. *Sens. Actuators B Chem.* **2019**, *279*, 148−156.
(18) Hofmockel, R.; Zschieschang, U.; Kraft, U.; Rödel, R.; Hansen, N. H.; Stolte, M.; Würthner, F.; Takimiya, K.; Kern, K.; Pflaum, J.; Klauk, H. High-Mobility Organic Thin-Film Transistors Based on a Small-Molecule Semiconductor Deposited in Vacuum and by Solution Shearing. *Org. Electron.* **2013**, *14* (12), 3213−3221.
(19) Tello, M.; Chiesa, M.; Duffy, C. M.; Sirringhaus, H. Charge Trapping in Intergrain Regions of Pentacene Thin Film Transistors. *Adv. Funct. Mater.* **2008**, *18* (24), 3907−3913.
(20) Park, S.; Kim, S. H.; Choi, H. H.; Kang, B.; Cho, K. Recent Advances in the Bias Stress Stability of Organic Transistors. *Adv. Funct. Mater.* **2020**, *30* (20), 1904590.
(21) Wünsche, J.; Deng, Y.; Kumar, P.; Di Mauro, E.; Josberger, E.; Sayago, J.; Pezzella, A.; Soavi, F.; Cicoira, F.; Rolandi, M.; Santato, C. Protonic and Electronic Transport in Hydrated Thin Films of the Pigment Eumelanin. *Chem. Mater.* **2015**, *27* (2), 436−442.
(22) Cramer, T.; Campana, A.; Leonardi, F.; Casalini, S.; Kyndiah, A.; Murgia, M.; Biscarini, F. Water-Gated Organic Field Effect Transistors − Opportunities for Biochemical Sensing and Extracellular Signal Transduction. *J. Mater. Chem. B* **2013**, *1* (31), 3728−3741.
(23) Haque, M. S.; Naseem, H. A.; Brown, W. D. The Effects of Moisture on Strain Relief of Si−O Bonds in Plasma-Enhanced Chemical Vapor Deposited Silicon Dioxide Films. *J. Electrochem. Soc.* **1997**, *144* (9), 3265.
(24) Baumgärtner, H.; Fuenzalida, V.; Eisele, I. Ozone Cleaning of the Si-SiO2 System. *Appl. Phys. A: Mater. Sci. Process.* **1987**, *43* (3), 223−226.
(25) Wasserman, S. R.; Tao, Y. T.; Whitesides, G. M. Structure and Reactivity of Alkylsiloxane Monolayers Formed by Reaction of Alkyltrichlorosilanes on Silicon Substrates. *Langmuir* **1989**, *5* (4), 1074−1087.
(26) Seo, M.-H.; Yang, H.-H.; Choi, K.-W.; Lee, J.-S.; Yoon, J.-B. A Simple Breathing Rate-Sensing Method Exploiting a Temporarily Condensed Water Layer Formed on an Oxidized Surface. *Appl. Phys. Lett.* **2015**, *106* (5), 053701.

(27) Thiel, P. A.; Madey, T. E. The Interaction of Water with Solid Surfaces: Fundamental Aspects. *Surf. Sci. Rep.* **1987**, *7* (6), 211−385.
(28) Anderson, J. H.; Parks, G. A. Electrical Conductivity of Silica Gel in the Presence of Adsorbed Water. *J. Phys. Chem.* **1968**, *72* (10), 3662−3668.
(29) Ito, K.; Harada, M.; Yamada, N. L.; Kudo, K.; Aoki, H.; Kanaya, T. Water Distribution in Nafion Thin Films on Hydrophilic and Hydrophobic Carbon Substrates. *Langmuir* **2020**, *36* (43), 12830−12837.
(30) Lambert, A. G.; Davies, P. B.; Neivandt, D. J. Implementing the Theory of Sum Frequency Generation Vibrational Spectroscopy: A Tutorial Review. *Appl. Spectrosc. Rev.* **2005**, *40* (2), 103−145.
(31) Young, G. J. Interaction of Water Vapor with Silica Surfaces. *J. Colloid Sci.* **1958**, *13* (1), 67−85.
(32) Yang, J.; Meng, S.; Xu, L.; Wang, E. G. Water Adsorption on Hydroxylated Silica Surfaces Studied Using the Density Functional Theory. *Phys. Rev. B* **2005**, *71* (3), 035413.
(33) Asay, D. B.; Kim, S. H. Evolution of the Adsorbed Water Layer Structure on Silicon Oxide at Room Temperature. *J. Phys. Chem. B* **2005**, *109* (35), 16760−16763.
(34) Kreuer, K. D. On the Complexity of Proton Conduction Phenomena. *Solid State Ion.* **2000**, *136*−*137*, 149−160.
(35) Schaefer, J. A.; Stucki, F.; Frankel, D. J.; Göpel, W.; Lapeyre, G. J. Adsorption of H, O, and H2O at Si(100) and Si(111) Surfaces in the Monolayer Range: A Combined EELS, LEED, and XPS Study. *J. Vac. Sci. Technol. B Microelectron. Process. Phenom.* **1984**, *2* (3), 359−365.
(36) Bhattacharyya, A.; Sanyal, M. K.; Mogera, U.; George, S. J.; Mukhopadhyay, M. K.; Maiti, S.; Kulkarni, G. U. In-Situ GISAXS Study of Supramolecular Nanofibers Having Ultrafast Humidity Sensitivity. *Sci. Rep.* **2017**, *7* (1), 246.
(37) Merces, L.; de Oliveira, R. F.; Gomes, H. L.; Bof Bufon, C. C. The Role of the Electrode Configuration on the Electrical Properties of Small-Molecule Semiconductor Thin-Films. *Org. Electron.* **2017**, *49*, 107−113.
(38) Paul, D. K.; McCreery, R.; Karan, K. Proton Transport Property in Supported Nafion Nanothin Films by Electrochemical Impedance Spectroscopy. *J. Electrochem. Soc.* **2014**, *161* (14), F1395.
(39) Paulsen, B. D.; Tybrandt, K.; Stavrinidou, E.; Rivnay, J. Organic Mixed Ionic−Electronic Conductors. *Nat. Mater.* **2020**, *19* (1), 13−26.
(40) Huggins, R. A. Simple Method to Determine Electronic and Ionic Components of the Conductivity in Mixed Conductors a Review. *Ionics* **2002**, *8* (3), 300−313.
(41) Patel, S. N.; Javier, A. E.; Stone, G. M.; Mullin, S. A.; Balsara, N. P. Simultaneous Conduction of Electronic Charge and Lithium Ions in Block Copolymers. *ACS Nano* **2012**, *6* (2), 1589−1600.
(42) Kreuer, K.-D.; Paddison, S. J.; Spohr, E.; Schuster, M. Transport in Proton Conductors for Fuel-Cell Applications: Simulations, Elementary Reactions, and Phenomenology. *Chem. Rev.* **2004**, *104* (10), 4637−4678.
(43) Mai, J.; Tang, N.; He, W.; Zou, Z.; Luo, C.; Zhang, A.; Fan, Z.; Wu, S.; Zeng, M.; Gao, J.; Zhou, G.; Lu, X.; Liu, J.-M. Effects of Ambient Gases on the Electrical Performance of Solution-Processed C8-BTBT Thin-Film Transistors. *Nanoscale Res. Lett.* **2019**, *14* (1), 169.
(44) Erdamar, O.; Skarlatos, Y.; Aktas, G.; Inci, M. N. Experimental Investigation of the Humidity Induced Change in the Conduction Mechanism of PEG. *Appl. Phys. A: Mater. Sci. Process.* **2006**, *83* (1), 159−162.
(45) Herranen, J. Characterisation of Poly(Ethylene Oxide) Sulfonic Acids. *Solid State Ion.* **1995**, *80* (3−4), 201−212.
(46) Chang, H. Y.; Thangamuthu, R.; Lin, C. W. Structure−Property Relationships in PEG/SiO2 Based Proton Conducting Hybrid Membranes—A 29Si CP/MAS Solid-State NMR Study. *J. Membr. Sci.* **2004**, *228* (2), 217−226.
(47) Park, Y.; Nagai, M. Proton-Conducting Properties of Inorganic-Organic Nanocomposites Proton-Exchange Nanocomposite Membranes Based on 3-Glycidoxypropyltrimethoxysilane and Tetraethylorthosilicate. *J. Electrochem. Soc.* **2001**, *148* (6), A616.
(48) Nagao, Y. Progress on Highly Proton-Conductive Polymer Thin Films with Organized Structure and Molecularly Oriented Structure. *Sci. Technol. Adv. Mater.* **2020**, *21* (1), 79−91.
(49) Baird, J. A.; Olayo-Valles, R.; Rinaldi, C.; Taylor, L. S. Effect of Molecular Weight, Temperature, and Additives on the Moisture Sorption Properties of Polyethylene Glycol. *J. Pharm. Sci.* **2010**, *99* (1), 154−168.
(50) Bilen, B.; Skarlatos, Y.; Aktas, G.; Inci, M. N.; Dispinar, T.; Kose, M. M.; Sanyal, A. In Situ Measurement of Humidity Induced Changes in the Refractive Index and Thickness of Polyethylene Glycol Thin Films. *J. Appl. Phys.* **2007**, *102* (7), 073534.

https://doi.org/10.1021/jacs.1c10119
J. Am. Chem. Soc. 2022, 144, 2546−2555